Design and analysis of active power control strategies for distributed generation inverters under unbalanced grid faults

Published in IET Generation, Transmission & Distribution
Received on 27th October 2009
Revised on 19th April 2010
doi: 10.1049/iet-gtd.2009.0607

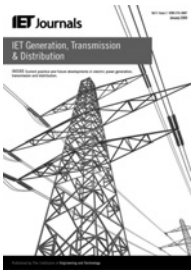

ISSN 1751-8687

Design and analysis of active power control strategies for distributed generation inverters under unbalanced grid faults

F. Wang J.L. Duarte M.A.M. Hendrix

Department of Electrical Engineering, Eindhoven University of Technology, Eindhoven 5600MB, The Netherlands
E-mail: f.wang@tue.nl

Abstract: Distributed power generation systems are expected to deliver active power into the grid and support it without interruption during unbalanced grid faults. Aiming to provide grid-interfacing inverters the flexibility to adapt to the coming change of grid requirements, an optimised active power control strategy is proposed to operate under grid faults. Specifically, through an adjustable parameter it is possible to change the relative amplitudes of oscillating active and reactive power smoothly, while simultaneously eliminating the second-order active or reactive power ripple at the two extremes of the parameter range. The steering possibility of the proposed strategy enables distributed generation inverters to be optimally designed from the perspectives of both the power-electronic converters and the power system. The proposed strategy is proved through simulation and further validated by experimental results.

1 Introduction

Voltage dips are short-duration decreases in rms voltage, usually caused by remote grid faults in the power system [1, 2]. Because most voltage dips are due to unbalanced faults, balanced voltage dips are relatively rare in practice. As shown in Fig. 1, a distributed generation (DG) system (three wire or four wire) is connected to the grid. A fault occurring in a parallel feeder will cause a voltage dip on the bus until a protection action trips to clear the fault. Conventionally, a transformer-isolated inverter would be required to disconnect from the grid when voltage dips and reconnect to the grid when faults are cleared. However, this requirement is changing. With the increasing application of renewable energy sources, more and more DG systems deliver electricity into the grid. Wind power generation, in particular, becomes an important electricity source in many countries. Consequently, grid codes now require wind energy systems to ride through voltage dips without interruption in order to maintain power delivery and to support the grid [3, 4]. Therefore it is necessary to investigate the ride-through control of wind turbine systems and other DG systems as well. Disregarding various upstream distributed sources and their controls, this paper will focus on the control of DG inverters.

Concerning the control of DG inverters under grid faults, two aspects should be noticed. First, fast system dynamics and good reference tracking are necessary. Note that inverters use the same converter topologies as pulse-width modulation (PWM) rectifiers. Hence, techniques that have been developed to control PWM rectifiers [5–9] can also be adapted to DG inverters. It has been shown that, because conventional controllers cannot effectively handle the negative-sequence voltages, systems under unbalanced voltage dips can have unbalanced and distorted grid currents as well as voltage variations in the dc bus [5]. This problem is discussed in [6], where dual PI current controllers in dual synchronous rotating frames (SRF) are proposed to control positive-sequence and negative-sequence components separately. Unfortunately, the symmetric sequences of feedback quantities have to be extracted in dc form by filtering out the components oscillating at twice the grid frequency. The system dynamics are considerably limited because of the notch filter used for this purpose. As an alternative, a delayed signal cancellation method with 1/4 fundamental period delay can be used to improve the sequence detection, but because of the time delay this method still influences the system dynamics [7, 8]. In order to leave out the sequence detection of feedback currents and

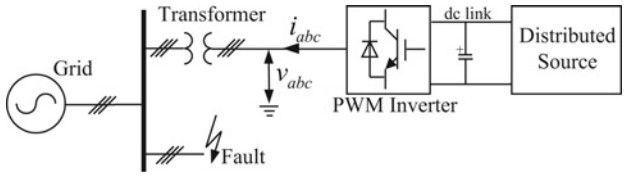

Figure 1 *DG inverter operates under grid faults*

further improve system dynamics, two extra resonant controllers working at twice the grid frequency are added to dual SRFs, eliminating the oscillation parts by means of compensation [9]. Alternatively, stationary frame resonant controllers are found to be suitable to control all the sequences (including the zero sequence that has been disregarded in many studies). This can simplify dual SRFs to a single stationary frame and achieve zero steady-sate error [10–12]. Also, symmetric sequence detection in feedback currents becomes unnecessary when using the resonant controllers, for example the scalar resonant control structure presented in [13]. In summary, in order to improve system dynamics and reference tracking, controllers must be able to deal with all the symmetric-sequence components and have direct feedback signals for closed-loop control. This is achieved by the controller employed in this paper.

Second, the generation of reference currents in case of unbalanced voltage dips is important. Assuming controllers are fast enough when voltage dips, then the only difference before and after a grid fault is a change in demanded current. Depending on practical applications, current reference generation is objective oriented. Considering the power-electronics converter constraints, a constant dc-link voltage is usually desirable, as in the objective set of [9, 14]. In other words, the instantaneous power at the output terminal of the inverter bridge is expected to be a constant. For simplification, only the instantaneous power at the grid connection point is considered by neglecting the part of oscillating power on account of the output filters [6]. However, a constant dc bus is achieved at the cost of unbalanced grid currents, and this results in a decrease of maximum deliverable power. In [15], a power reducing scheme is used to confine the current during a grid fault. On the other hand, the affects of the grid currents on the power system side should also be taken into account when designing reference currents for DG inverters. As presented in [16], several individual strategies are possible to obtain different power quality at the grid connection point in terms of instantaneous power oscillation and current distortion. These strategies show flexible control possibilities of DG systems under grid faults. However, they only cope with specific cases. Therefore starting from the ideas in [16], a generalised strategy on reference current generation is designed. Further discussion and analysis based on this strategy are also carried out in this paper.

This paper presents a generalised active power control strategy under unbalanced grid faults based on symmetric-sequence components and shows explicitly the contributions of symmetrical sequences to instantaneous power. The steering possibility of the proposed strategy enables DG inverters to be optimally designed from the perspectives of both the power-electronics converters and the grid. Thus, a further discussion on objective-oriented optimisations of the proposed strategy is presented. A stationary frame resonant controller with direct feedback variables is employed to construct a dual-loop control structure. In addition, feed-forward of the grid voltage is added to help improving system response to grid disturbances. Based on this control structure, simulations and experiments are carried out to validate the proposed strategy.

2 Instantaneous power calculation

In this section, the instantaneous power theory [17, 18] is revisited. Then instantaneous power calculation based on symmetric sequences is developed, and the notation for the reference current design in the next sections is defined.

2.1 Instantaneous power theory

For a three-phase DG system shown in Fig. 1, instantaneous active power and reactive power at the grid connection point are given by, respectively

$$p = \boldsymbol{v} \cdot \boldsymbol{i} = v_a i_a + v_b i_b + v_c i_c \tag{1}$$

$$q = \boldsymbol{v}_\perp \cdot \boldsymbol{i} = \frac{1}{\sqrt{3}}[(v_a - v_b)i_c + (v_b - v_c)i_a + (v_c - v_a)i_b]$$

$$\text{with} \quad \boldsymbol{v}_\perp = \frac{1}{\sqrt{3}}\begin{bmatrix} 0 & 1 & -1 \\ -1 & 0 & 1 \\ 1 & -1 & 0 \end{bmatrix}\boldsymbol{v} \tag{2}$$

where $\boldsymbol{v} = [\,v_a \quad v_b \quad v_c\,]^{\mathrm{T}}$, $\boldsymbol{i} = [\,i_a \quad i_b \quad i_c\,]^{\mathrm{T}}$, bold-italic symbols represent vectors, and the operator '$\cdot$' denotes the dot product of vectors. Note that the subscript '$\perp$' is used to represent a vector derived from the matrix transformation in (2), although vectors $\boldsymbol{v}_\perp$ and $\boldsymbol{v}$ are orthogonal only when the three-phase components in vector $\boldsymbol{v}$ are balanced.

To deliver a given constant instantaneous active power ($p = P$) and zero reactive power, the corresponding currents can be calculated based on the instantaneous power theory. The derived currents, denoted by $\boldsymbol{i}_p$, are expressed by

$$\boldsymbol{i}_p = \frac{P}{\|\boldsymbol{v}\|^2}\boldsymbol{v} \tag{3}$$

where $\|\boldsymbol{v}\|^2 = \boldsymbol{v} \cdot \boldsymbol{v} = v_a^2 + v_b^2 + v_c^2$, operator '$\|\cdot\|$' means the norm of a vector, and subscript 'p' represents active power-related quantities. Since $\boldsymbol{i}_p$ is in phase with $\boldsymbol{v}$, the resulting instantaneous reactive power q in (2) equals zero. Because

doi: 10.1049/iet-gtd.2009.0607

$\|\boldsymbol{v}\|$ is constant when the voltages are balanced and sinusoidal, the derived currents are also balanced and sinusoidal waveforms. However, when the voltages become unbalanced or distorted, $\|\boldsymbol{v}\|$ is not a constant but varies with twice the fundamental frequency. Consequently, reference current $\boldsymbol{i}_p$ becomes distorted and unbalanced, as illustrated in Fig. 2.

Although the method of instantaneous power control achieves constant active and reactive power at the cost of current distortion, it may not be acceptable to inject low-quality currents into the grid even during voltage dips. It is conceivable to employ only balanced fundamental quantities for sinusoidal current generation. Therefore instantaneous power calculations based on symmetric-sequence components is derived in the following.

2.2 Symmetric-sequence based instantaneous power

Phasor notation is a proven and convenient way to describe sinusoidal quantities. For instance, where harmonics are negligible, voltages in the $a-b-c$ frame can be expressed by

$$\boldsymbol{v} = \begin{bmatrix} v_a \\ v_b \\ v_c \end{bmatrix} = \Re\left(\mathrm{e}^{\mathrm{j}\omega t} \begin{bmatrix} \underline{V}_a \\ \underline{V}_b \\ \underline{V}_c \end{bmatrix} \right) \tag{4}$$

where phasors are denoted with a bar subscript, and $\Re(\cdot)$ represents the real part of a complex number. Applying symmetric-components transformation [19] to voltage phasors yields symmetric-sequence phasors as

$$\begin{bmatrix} \underline{V}^0 \\ \underline{V}^+ \\ \underline{V}^- \end{bmatrix} = \frac{1}{3} \begin{bmatrix} 1 & 1 & 1 \\ 1 & a & a^2 \\ 1 & a^2 & a \end{bmatrix} \begin{bmatrix} \underline{V}_a \\ \underline{V}_b \\ \underline{V}_c \end{bmatrix}, \quad \text{with } a = \mathrm{e}^{\mathrm{j}(2\pi/3)} \tag{5}$$

where subscripts '+', '−', and '0' denote positive, negative and zero sequences, respectively. The inverse transformation of (5) is found to be

$$\begin{bmatrix} \underline{V}_a \\ \underline{V}_b \\ \underline{V}_c \end{bmatrix} = \begin{bmatrix} 1 & 1 & 1 \\ 1 & a^2 & a \\ 1 & a & a^2 \end{bmatrix} \begin{bmatrix} \underline{V}^0 \\ \underline{V}^+ \\ \underline{V}^- \end{bmatrix} \tag{6}$$

Correspondingly, instantaneous values can be derived from the symmetric-component phasors given by (6). Otherwise stated, the following expressions for the $a-b-c$ voltages are applicable

$$\boldsymbol{v} = \boldsymbol{v}^+ + \boldsymbol{v}^- + \boldsymbol{v}^0 \tag{7}$$

where

$$\boldsymbol{v}^+ = \begin{bmatrix} v_a^+ \\ v_b^+ \\ v_c^+ \end{bmatrix} = \Re\left(\underline{V}^+ \mathrm{e}^{\mathrm{j}\omega t} \begin{bmatrix} 1 \\ a^2 \\ a \end{bmatrix} \right)$$

$$\boldsymbol{v}^- = \begin{bmatrix} v_a^- \\ v_b^- \\ v_c^- \end{bmatrix} = \Re\left(\underline{V}^- \mathrm{e}^{\mathrm{j}\omega t} \begin{bmatrix} 1 \\ a \\ a^2 \end{bmatrix} \right)$$

$$\boldsymbol{v}^0 = \begin{bmatrix} v_a^0 \\ v_b^0 \\ v_c^0 \end{bmatrix} = \Re\left(\underline{V}^0 \mathrm{e}^{\mathrm{j}\omega t} \begin{bmatrix} 1 \\ 1 \\ 1 \end{bmatrix} \right)$$

Similarly, current quantities can also be represented in terms of symmetric sequences, that is

$$\boldsymbol{i} = \boldsymbol{i}^+ + \boldsymbol{i}^- + \boldsymbol{i}^0 \tag{8}$$

where $\boldsymbol{i}^{+,-,0} = \begin{bmatrix} i_a^{+,-,0} & i_b^{+,-,0} & i_c^{+,-,0} \end{bmatrix}^{\mathrm{T}}$. As a result, the calculation of instantaneous power in (1) and (2) can be rewritten as

$$p = \boldsymbol{v} \cdot \boldsymbol{i} = (\boldsymbol{v}^+ + \boldsymbol{v}^- + \boldsymbol{v}^0) \cdot (\boldsymbol{i}^+ + \boldsymbol{i}^- + \boldsymbol{i}^0) \tag{9}$$

$$q = \boldsymbol{v}_\perp \cdot \boldsymbol{i} = (\boldsymbol{v}_\perp^+ + \boldsymbol{v}_\perp^- + \boldsymbol{v}_\perp^0) \cdot (\boldsymbol{i}^+ + \boldsymbol{i}^- + \boldsymbol{i}^0) \tag{10}$$

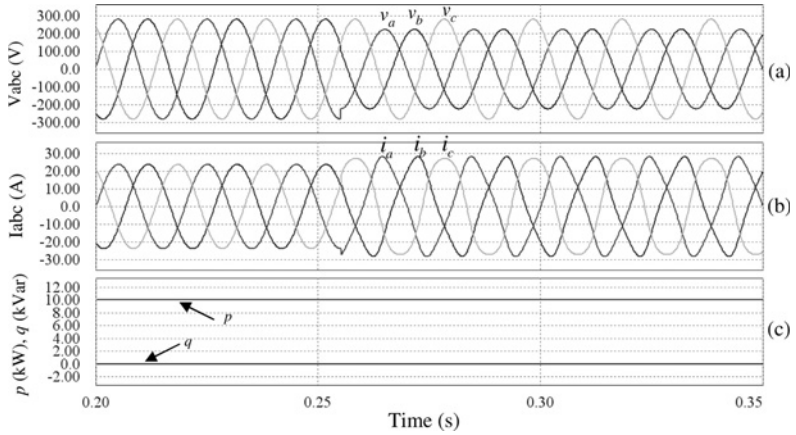

Figure 2 *Simulation results obtained based on instantaneous power theory*

a Phase voltages, where voltages of phase *a* and *b* dip to 80% at $t = 0.255$ s
b Injected currents
c Instantaneous *p*, *q*

With respect to the definitions of the symmetric-sequence vector in (7), corresponding orthogonal vectors in (10) can be derived by using the matrix transformation in (2). Note that $\boldsymbol{v}_{\perp}^{+}$ lags $\boldsymbol{v}^{+}$ by 90^0, $\boldsymbol{v}_{\perp}^{-}$ leads $\boldsymbol{v}^{-}$ by 90^0 and $\boldsymbol{v}_{\perp}^{0}$ is always equal to zero. Because the dot products between $\boldsymbol{i}^0$ and positive-sequence or negative-sequence voltage vectors are also always zero (because symmetry of the components in $\boldsymbol{v}^{+}$ and $\boldsymbol{v}^{-}$), equations (9) and (10) can be simplified by

$$p = \boldsymbol{v} \cdot \boldsymbol{i} = (\boldsymbol{v}^{+} + \boldsymbol{v}^{-}) \cdot (\boldsymbol{i}^{+} + \boldsymbol{i}^{-}) + \boldsymbol{v}^{0} \cdot \boldsymbol{i}^{0} \tag{11}$$

$$q = \boldsymbol{v}_{\perp} \cdot \boldsymbol{i} = (\boldsymbol{v}_{\perp}^{+} + \boldsymbol{v}_{\perp}^{-}) \cdot (\boldsymbol{i}^{+} + \boldsymbol{i}^{-}) \tag{12}$$

Because the calculation of instantaneous power and current references is carried out in terms of vectors, it can also be used in other reference frames, simply by substituting the vectors in the a–b–c frames with vectors derived in other frames, for example, the stationary α–β–γ reference frame (see Appendix 1). Note that in the experiment these symmetric-sequence components are detected in the time domain. Based on this symmetric-sequence-based power definition, a comprehensive investigation on how to generate sinusoidal current references for DG inverters is presented in the next section.

3 Design generalised current reference generation

In this section, current control based only on positive-sequence and negative-sequence components is investigated. Because zero-sequence voltages of unbalanced voltage dips do not exist in three-wire systems, nor can they propagate to the secondary side of star-ungrounded or delta connected transformers in four-wire systems, most case-studies only consider positive and negative sequences. Even for unbalanced systems with zero-sequence voltage, four-leg inverter topologies can eliminate zero-sequence current with appropriate control, as tested in the experiments, and no power introduced by zero-sequence components exists.

Simplifying assumptions we will use:

- Only positive-sequence and negative-sequence currents are present;
- Only fundamental components exist, the power introduced by harmonics is vanishingly small; and
- The amplitude of the positive-sequence voltage is higher than the negative sequence, that is $\|\boldsymbol{v}^{+}\| > \|\boldsymbol{v}^{-}\|$.

Since no zero-sequence currents are involved, $\boldsymbol{i}_p$ can be separated into $\boldsymbol{i}_p^{+}$ and $\boldsymbol{i}_p^{-}$, which will be defined in phase with $\boldsymbol{v}^{+}$ and $\boldsymbol{v}^{-}$, respectively, in order to yield active power only. Rewriting (11) and (12) in terms of $\boldsymbol{i}_p^{+}$ and $\boldsymbol{i}_p^{-}$, we obtain

$$p = \underbrace{\boldsymbol{v}^{+} \cdot \boldsymbol{i}_p^{+}}_{P^{+}} + \underbrace{\boldsymbol{v}^{-} \cdot \boldsymbol{i}_p^{-}}_{P^{-}} + \underbrace{\boldsymbol{v}^{+} \cdot \boldsymbol{i}_p^{-} + \boldsymbol{v}^{-} \cdot \boldsymbol{i}_p^{+}}_{\tilde{p}_{2\omega}} \tag{13}$$

$$q = \underbrace{\boldsymbol{v}_{\perp}^{-} \cdot \boldsymbol{i}_p^{+} + \boldsymbol{v}_{\perp}^{+} \cdot \boldsymbol{i}_p^{-}}_{\tilde{q}_{2\omega}} \tag{14}$$

where P^{+} and P^{-} denote the constant active power introduced by positive and negative sequences, respectively $\tilde{p}_{2\omega}$ is oscillating active power and $\tilde{q}_{2\omega}$ oscillating reactive power. It can be found that the two terms of $\tilde{p}_{2\omega}$ are in-phase quantities oscillating at twice the fundamental frequency (see Appendix 2). A similar property can be found for the two terms of $\tilde{q}_{2\omega}$.

Because oscillating active power can reflect a variation on the dc-link voltage, and high dc-voltage variation may cause over-voltage problems, output distortion, or even control instability, it is desirable to eliminate $\tilde{p}_{2\omega}$. On the other hand, the oscillating reactive power $\tilde{q}_{2\omega}$ also causes power losses and operating current rise, and therefore it is advantageous to mitigate $\tilde{q}_{2\omega}$ as well. A trade-off between $\tilde{p}_{2\omega}$ and $\tilde{q}_{2\omega}$ is not straightforward and depends on practical requirements. In the following, strategies to achieve controllable oscillating active and reactive power are derived from two considerations.

3.1 Controllable oscillating active power

For given power P, which is determined by the power of DG sources and system power ratings, the first two terms of (13) are designed to meet

$$P = \boldsymbol{v}^{+} \cdot \boldsymbol{i}_p^{+} + \boldsymbol{v}^{-} \cdot \boldsymbol{i}_p^{-} \tag{15}$$

Since the two terms of $\tilde{p}_{2\omega}$ in (13) are in-phase quantities that add to each other, it is expected that these two terms can compensate each other. By setting intentionally

$$\boldsymbol{v}^{+} \cdot \boldsymbol{i}_p^{-} = -k_p \boldsymbol{v}^{-} \cdot \boldsymbol{i}_p^{+}, \quad 0 \le k_p \le 1 \tag{16}$$

after some manipulations the negative-sequence current $\boldsymbol{i}_p^{-}$ is derived from (16) as

$$\boldsymbol{i}_p^{-} = \frac{-k_p \boldsymbol{v}^{+} \cdot \boldsymbol{i}_p^{+}}{\|\boldsymbol{v}^{+}\|^2} \boldsymbol{v}^{-} \tag{17}$$

Substituting (17) into (15), we obtain

$$P\|\boldsymbol{v}^{+}\|^2 = (\|\boldsymbol{v}^{+}\|^2 - k_p\|\boldsymbol{v}^{-}\|^2)(\boldsymbol{v}^{+} \cdot \boldsymbol{i}_p^{+}) \tag{18}$$

Then, based on (17) and (18), currents $\boldsymbol{i}_p^{+}$ and $\boldsymbol{i}_p^{-}$ can be

doi: 10.1049/iet-gtd.2009.0607

calculated as

$$\boldsymbol{i}_p^+ = \frac{P}{\|\boldsymbol{v}^+\|^2 - k_p\|\boldsymbol{v}^-\|^2}\boldsymbol{v}^+ \tag{19}$$

$$\boldsymbol{i}_p^- = \frac{-k_p P}{\|\boldsymbol{v}^+\|^2 - k_p\|\boldsymbol{v}^-\|^2}\boldsymbol{v}^- \tag{20}$$

Finally, the total current reference is the sum of $\boldsymbol{i}_p^+$ and $\boldsymbol{i}_p^-$, that is

$$\boldsymbol{i}_p^* = \frac{P}{\|\boldsymbol{v}^+\|^2 - k_p\|\boldsymbol{v}^-\|^2}(\boldsymbol{v}^+ - k_p\boldsymbol{v}^-), \quad 0 \le k_p \le 1 \tag{21}$$

3.2 Controllable oscillating reactive power

Instead of compensating the oscillating active power in (13), we can similarly shape the oscillating reactive power in (14). For this purpose negative-sequence currents are imposed to meet

$$\boldsymbol{v}_\perp^+ \cdot \boldsymbol{i}_p^- = -k_p\boldsymbol{v}_\perp^- \cdot \boldsymbol{i}_p^+, \quad 0 \le k_p \le 1 \tag{22}$$

By considering equation $\boldsymbol{v}_\perp^+ \cdot \boldsymbol{i}^- = -\boldsymbol{v}^+ \cdot \boldsymbol{i}_\perp^-$ (because $\boldsymbol{v}_\perp^+$ lags $\boldsymbol{v}^+$ by 90^0 and $\boldsymbol{i}_\perp^-$ leads $\boldsymbol{i}^-$ by 90^0), the left side of (22) can be rewritten as

$$\boldsymbol{v}_\perp^+ \cdot \boldsymbol{i}_p^- = -\boldsymbol{v}^+ \cdot \boldsymbol{i}_{p\perp}^- = -k_p\boldsymbol{v}_\perp^- \cdot \boldsymbol{i}_p^+ \tag{23}$$

where $\boldsymbol{i}_{p\perp}^-$ denotes the orthogonal vector of $\boldsymbol{i}_p^-$ according to (2). Then, it follows that

$$\boldsymbol{i}_{p\perp}^- = \frac{k_p\boldsymbol{v}^+ \cdot \boldsymbol{i}_p^+}{\|\boldsymbol{v}^+\|^2}\boldsymbol{v}_\perp^- \tag{24}$$

Hence the negative-sequence current $\boldsymbol{i}_p^-$ follows directly from (24) as

$$\boldsymbol{i}_p^- = \frac{k_p\boldsymbol{v}^+ \cdot \boldsymbol{i}_p^+}{\|\boldsymbol{v}^+\|^2}\boldsymbol{v}^- \tag{25}$$

Solving (15) and (25), the positive-sequence currents and negative-sequence currents are derived as

$$\boldsymbol{i}_p^+ = \frac{P}{\|\boldsymbol{v}^+\|^2 + k_p\|\boldsymbol{v}^-\|^2}\boldsymbol{v}^+ \tag{26}$$

$$\boldsymbol{i}_p^- = \frac{k_p P}{\|\boldsymbol{v}^+\|^2 + k_p\|\boldsymbol{v}^-\|^2}\boldsymbol{v}^- \tag{27}$$

Again, the total current reference is the sum of $\boldsymbol{i}_p^+$ and $\boldsymbol{i}_p^-$, that is

$$\boldsymbol{i}_p^* = \frac{P}{\|\boldsymbol{v}^+\|^2 + k_p\|\boldsymbol{v}^-\|^2}(\boldsymbol{v}^+ + k_p\boldsymbol{v}^-), \quad 0 \le k_p \le 1 \tag{28}$$

3.3 Combining strategies a and b

Simple analysis reveals that (21) and (22) can be combined and represented by

$$\boldsymbol{i}_p^* = \frac{P}{\|\boldsymbol{v}^+\|^2 + k_p\|\boldsymbol{v}^-\|^2}(\boldsymbol{v}^+ + k_p\boldsymbol{v}^-), \quad -1 \le k_p \le 1 \tag{29}$$

In order to analyse the variation of the power, we substitute (29) into (13) and (14), and the results are

$$p = P + \frac{P(1+k_p)(\boldsymbol{v}^- \cdot \boldsymbol{v}^+)}{\|\boldsymbol{v}^+\|^2 + k_p\|\boldsymbol{v}^-\|^2} \tag{30}$$

$$q = \frac{P(1-k_p)(\boldsymbol{v}_\perp^- \cdot \boldsymbol{v}^+)}{\|\boldsymbol{v}^+\|^2 + k_p\|\boldsymbol{v}^-\|^2} \tag{31}$$

It can be seen that the variant terms of (30) and (31), that is oscillating active power and reactive power, are controlled by the coefficient k_p. These two parts of oscillating power are orthogonal and equal in maximum amplitude. Simulation results are obtained in Fig. 3 by sweeping the parameter k_p. Related circuit structure and controller parameters are given in the experimental part. It can be seen that either oscillating active power or oscillating reactive power can be controlled and even can be eliminated at the two extremes of the k_p curve. In other words, a constant dc-link voltage can be achieved because of the elimination of oscillating active power when $k_p = -1$; symmetric currents can be derived when $k_p = 0$; and unity power factor can be achieved when $k_p = 1$ where the three-phase currents follows the grid voltages. Therefore infinite points of k_p between -1 and 1 will allow a optimum control of the currents in order to achieve different objectives. For instance, within a certain range of dc-voltage variation, the currents can be optimised to get maximum power output by changing the k_p with respect to the grid voltages. More discussions on the choices of k_p are presented in the next section. Furthermore, a graphic representation of the relationship between these two instantaneous oscillating power is plotted in Fig. 4*a*. It illustrates clearly that these two part of oscillating power shift from one to another with the increase or decrease of k_p under the proposed strategy. This controllable characteristic allows to enhance system control flexibility and facilitates system optimisation. Further discussion on objective-oriented optimisations of this generalised strategy will be presented in the next section.

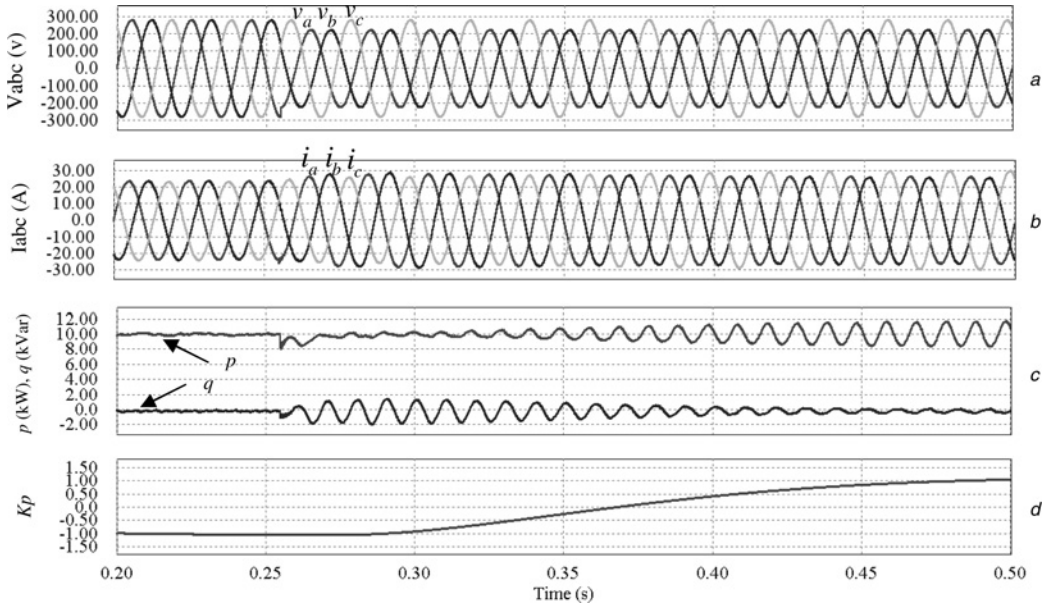

Figure 3 *Simulation results of the proposed control strategy*

a Phase voltages, where voltages of phase *a* and *b* dip to 80% at $t = 0.255$ s
b Injected currents
c Instantaneous *p*, *q*
d Controllable coefficient k_p sweeping from -1 to 1

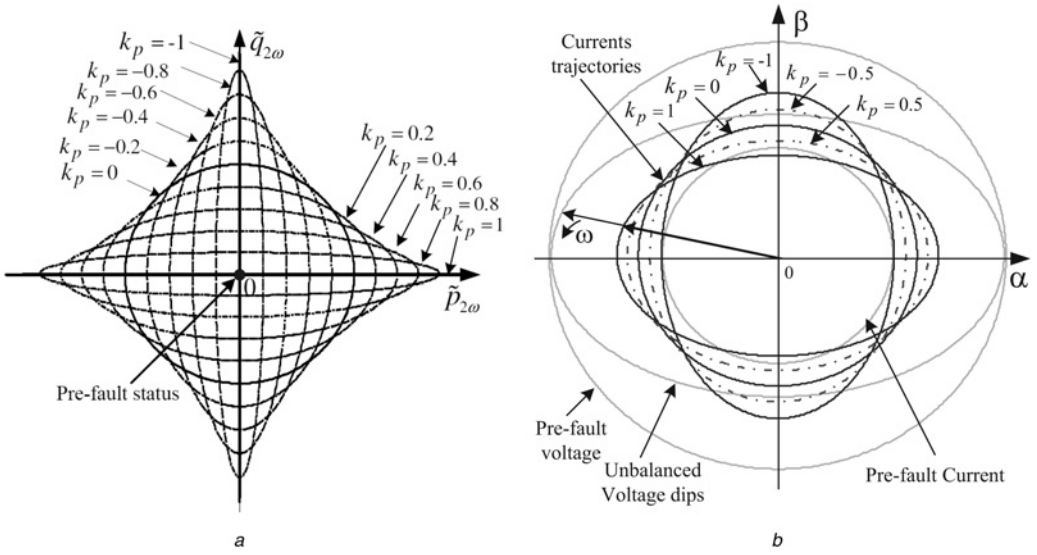

Figure 4 *Graphic representation*

a Relationship between oscillating active power $\tilde{p}_{2\omega}$ and oscillating reactive power $\tilde{q}_{2\omega}$
b Grid voltage and current trajectories before and after unbalanced voltage dips in the stationary frame, with k_p as a changing parameter

4 Analysis on strategy applications

As can be observed, the proposed current reference generation strategy provides DG inverters control flexibility, that is the coefficient k_p can be optimally determined based on optimisation objectives and be adaptively changed in case of voltage dips. Therefore the applications of the proposed strategy are discussed from different aspects.

4.1 Constraints of DG inverters

Considering the power-electronic converter constraints, a serious problem for the inverters is the second-order ripple on the dc bus, which reflects to the ac side and creates distorted grid currents during unbalanced voltage dips. Either for facilitating dc-bus voltage control or for minimising the dc-bus capacitors, it is preferred to make k_p in (29) close to -1 so that the dc-voltage variations can be kept very small. However, the maximum deliverable power

doi: 10.1049/iet-gtd.2009.0607

has to decrease because unbalanced phase currents reduce the operating margin of inverters. Therefore for a maximum power-tracking system it is preferable to shift k_p towards zero to get balanced currents as long as the variation on dc link is acceptable. Note that the inverter losses and oscillating power on account of output filters are not considered, whereas the effects of output filters will be commented on later.

To help understanding, a vector diagram that represents current trajectories changing with k_p under an unbalanced voltage dip is drawn in Fig. 4*b*. For a desired power P, unbalanced currents are generated to achieve zero $\tilde{p}_{2\omega}$ when k_p equals -1. When the asymmetry of voltage dips become more pronounced, the generated currents will finally cross overcurrent levels if the system tries to maintain the same power delivery as during the pre-fault status and keeps zero $\tilde{p}_{2\omega}$ simultaneously. Therefore k_p has to be adapted towards zero, as shown in Fig. 4*b*, that is the current trajectory starts from the flattest ellipse and reshapes to a circle. Hence, k_p will be somewhere in between 0 and 1 as long as $\tilde{p}_{2\omega}$ is smaller than the allowed maximum value $\tilde{p}_{2\omega\_\max}$, which can be calculated by

$$\tilde{p}_{2\omega\_\max} = 2\pi f\, V_{\mathrm{dc}} C_{\mathrm{dc}} \Delta V_{\mathrm{dc}} \tag{32}$$

where f is the grid frequency, V_{dc} is the average dc voltage, C_{dc} is the dc-link capacitance and ΔV_{dc} the specified dc-voltage variation. Note that when k_p reaches zero and the amplitudes of balanced currents are still out of the maximum current range, the delivered power has to be decreased. As a consequence, the upstream distributed sources should also take actions to guarantee the power balance on the dc link.

4.2 Effects on the grid

On the other hand, the effects of the proposed strategy on the power system side could also impose constraints on the control design, especially for large-scale DG systems. Because the oscillating reactive power causes extra power losses in the grid, it is preferred to make k_p close to 1 in order to eliminate $\tilde{q}_{2\omega}$. Again, the dc variation becomes a constraint because the amplitude of $\tilde{p}_{2\omega}$ is increasing when k_p shifts to 1. Therefore similar comparison between the predicted oscillating power given by (30) and $\tilde{p}_{2\omega\_\max}$ given by 32) should be carried out. As long as the active power oscillation is acceptable, k_p can move towards 1 as close as possible. Otherwise, delivered power downgrades in quantity.

However, the objective becomes different from voltage quality point of view. As shown in the results of Fig. 3, when k_p is getting close to 1, less current is delivered into the phases in which grid voltage is relatively low. Also, it can be seen in Fig. 4*b* that the current vector tends to synchronise with the grid voltage vector, that is the reference currents tend to follow the asymmetry of the grid voltages. Consequently, the unbalanced voltage will be worsened because unbalanced voltage rise across grid impedances, which is introduced by the injected grid currents (if the grid impedance is resistive and the injected currents are large enough). On the contrary, when k_p is close to -1, higher current is delivered into the phases in which grid voltage is relatively low, thereby compensating the voltage imbalance at the grid connection point. As is revealed in the analysis above, the objectives of improving the effects on the grid side could conflict with each other. Fortunately, the proposed strategy can be easily adapted according to practical objectives.

4.3 Effects of output inductors

The effects of output inductors are well known and therefore are shortly presented here. The instantaneous power control discussed so far has been treated at the grid connection point. When the objective is aimed at optimising dc-voltage variations, and the oscillating power on account of the output inductors cannot be neglected (in case of large and unbalanced currents or small dc capacitance), the fundamental components of the inverter-bridge output voltages should be used in the proposed strategy for calculation instead of the grid voltages. Indirect derivation based on grid voltages and currents or direct measurement on the output of inverter bridge can be used to get the voltages as presented in [9, 14].

5 Experimental verification

To verify the proposed strategy, experiments are carried out on a laboratory experimental system constructed from a four-leg inverter that is connected to the grid through LCL filters, as shown in Fig. 5. The system parameters are listed in Table 1. By using a four-leg inverter, zero-sequence currents can be eliminated when the grid has zero-sequence voltages. For the cases where the zero-sequence voltage of unbalanced grid dips is isolated by transformers, a three-leg inverter can be applied. A 15 kV A three-phase programmable ac-power source is used to emulate the unbalanced utility grid and the distributed source is implemented by a dc-power supply.

5.1 Control realisation

The controller is realised with a double-loop current controller, which consists of an outer control loop with proportional-resonant (PR) controllers for compensating the steady-state error of the fundamental-frequency currents and an inner inductor current control loop with simple proportional gain to improve stability. In addition, a feed-forward loop from the grid voltages is used to improve system response to voltage disturbances.

Furthermore, the direct feedback of currents in the stationary frame is achieved, which is desirable as presented in Section 1. Also, the control for dual sequence

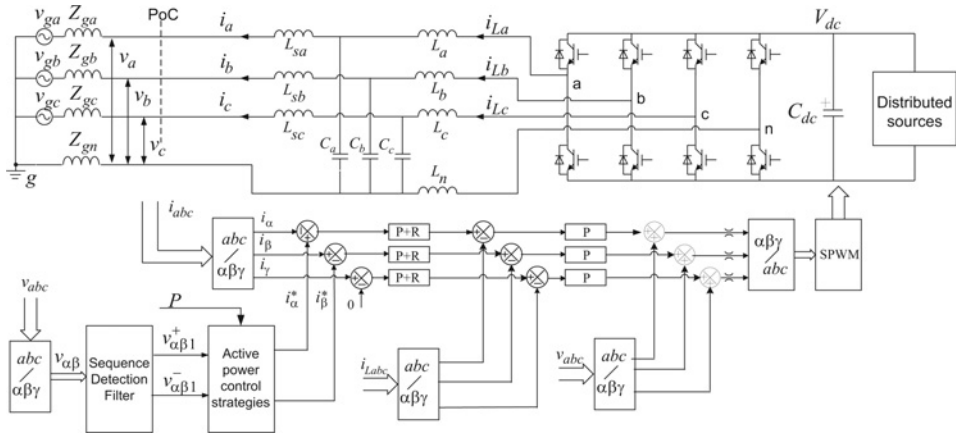

Figure 5 *Circuit diagram and control structure of experimental four-leg inverter system*

components would be simple without transformations between reference frames. A quasi-PR controller with high gain at the fundamental frequency is used

$$G_i(s) = K_p + \frac{2K_r\omega_{br}s}{s^2 + 2\omega_{br}s + \omega_1^2} \tag{33}$$

where K_p is the proportional gain, K_r is the resonant gain, ω_1 denotes the fundamental radian frequency and ω_{br} the equivalent bandwidth of the resonant controller. A detailed design for the PR controller and its application have been presented in [11, 12]. Through optimising, the parameters used in the experiment are $K_p = 2$, $K_r = 100$ and $\omega_{br} = 10$ rad/s.

The symmetric-sequence components are detected in the time domain with a stationary frame filter in the $\alpha-\beta$ frame [20]. The basic filter cell was demonstrated to be equivalent to a band-pass filter in the stationary frame, and can be easily implemented using a multi-state-variable structure shown in Fig. 6. Because of its robustness for small frequency variations, a phase locked loop (PLL) is avoided in this experiment since the power supply only emulates the magnitude drop of the grid voltage. Otherwise, a PLL should be added to the filter for adapting to large frequency changes [20].

Table 1 System parameters

Description	Symbol	Value
output filtering inductor	$L_{sa,b,c}$	2 mH
output filtering capacitor	$C_{a,b,c}$	5 μF
output filtering inductor	$L_{a,b,c}$	2 mH
neutral filtering inductor	L_n	0.67 mH
dC-link voltage	V_{dc}	750 V
dC-link capacitors	C_{dc}	4400 μF/900 V_{dc}
switching frequency	f_{sw}	16 kHz
system rated power	S	15 kVA
tested power	P	2500 W

5.2 Experimental results

By shifting the controllable parameter k_p, the system is tested under unbalanced voltage dips with the proposed strategy. In order to capture the transient reaction of the system, three situations are intentionally tested for comparison at the start moment and finish moment of voltage dips.

5.2.1 Under voltage dips: As shown in Fig. 7*a*, grid voltages are emulated to be faulty at $t = 0.03$ s where phases A and B dip to 80%. In case of $k_p = -1$, the injected grid currents and instantaneous power are shown in Fig. 8*a*. It can be seen that the currents on phases with lower voltage are higher than the phase with higher voltage in order to obtain a constant active power.

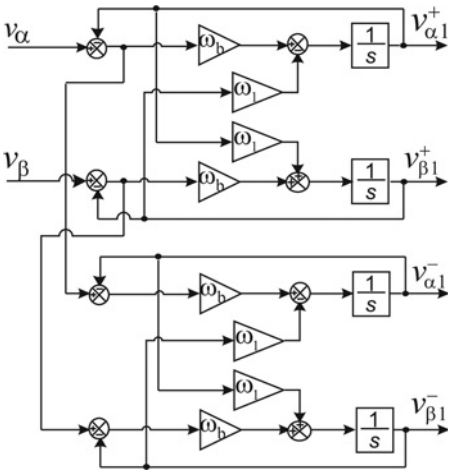

Figure 6 *Implementation diagram of sequence detection, where $\omega_1 = 314$ rad/s, $\omega_b = 100$ rad/s*

doi: 10.1049/iet-gtd.2009.0607

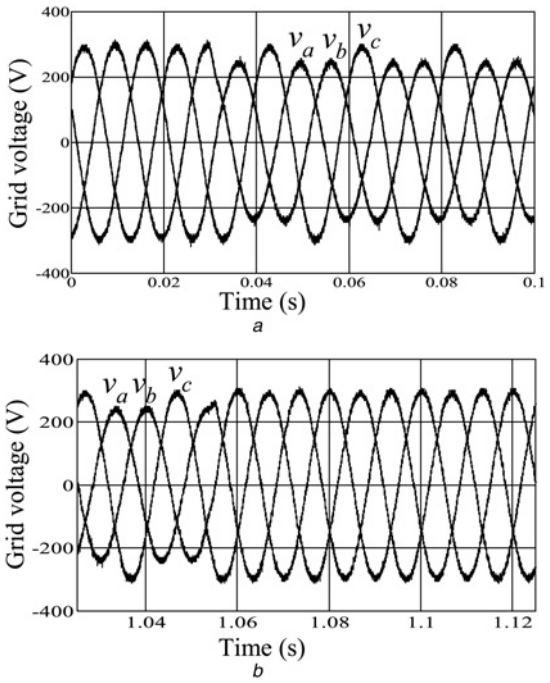

Figure 7 *Emulated grid voltages*

a To be faulty at $t = 0.03$ s, where phases *a* and *b* dip to 80%
b To be recovered at $t = 1.055$ s

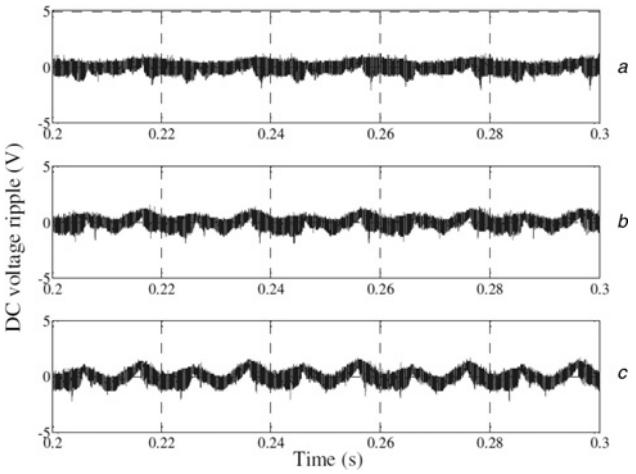

Figure 9 *Experimental results of dc-link ripple under unbalanced voltage*

a With $k_p = -1$
b With $k_p = 0$
c With $k_p = 1$

As analysed in Section 3, a set of negative-sequence current opposite to the negative-sequence voltage is injected to compensate the part of oscillating active power introduced by negative-sequence voltage and positive-sequence currents. Also, it can be seen that the instantaneous reactive power has a large power ripple oscillating at twice the grid frequency. The worst case is when $k_p = -1$ because of an extra part of oscillating reactive power generated by the negative-sequence currents and positive-sequence voltages.

In Fig. 8*b*, results with $k_p = 0$ are shown. As illustrated, the currents are kept balanced before and after grid faults. Hence, the oscillating part of the instantaneous active and reactive

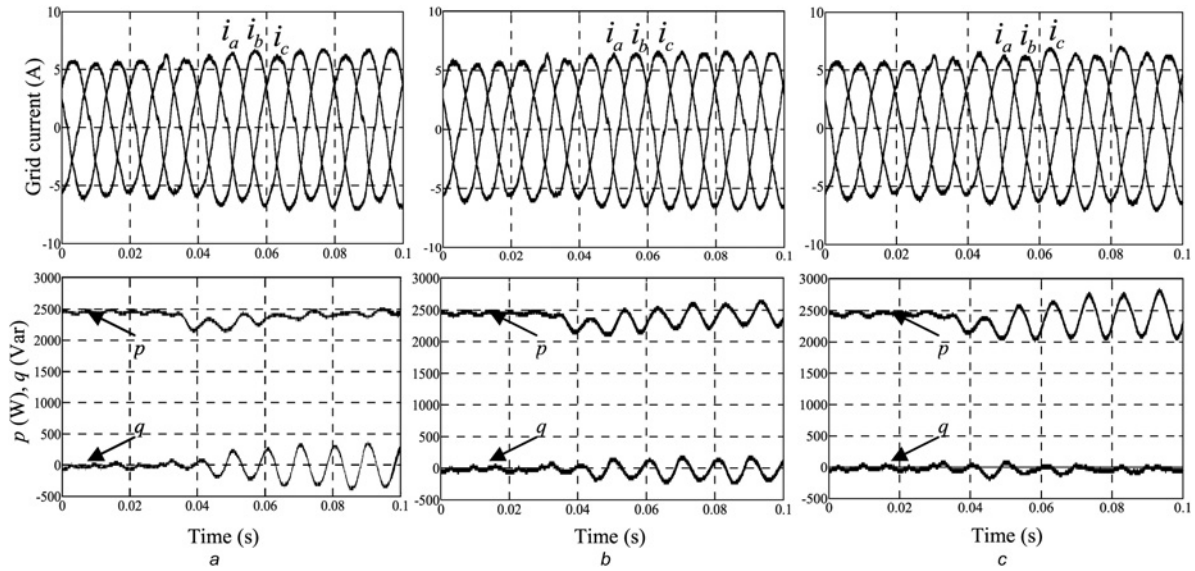

Figure 8 *Experimental results under unbalanced voltage dips, where the waveforms from top to bottom are injected grid currents and instantaneous power*

a With $k_p = -1$
b With $k_p = 0$
c With $k_p = 1$

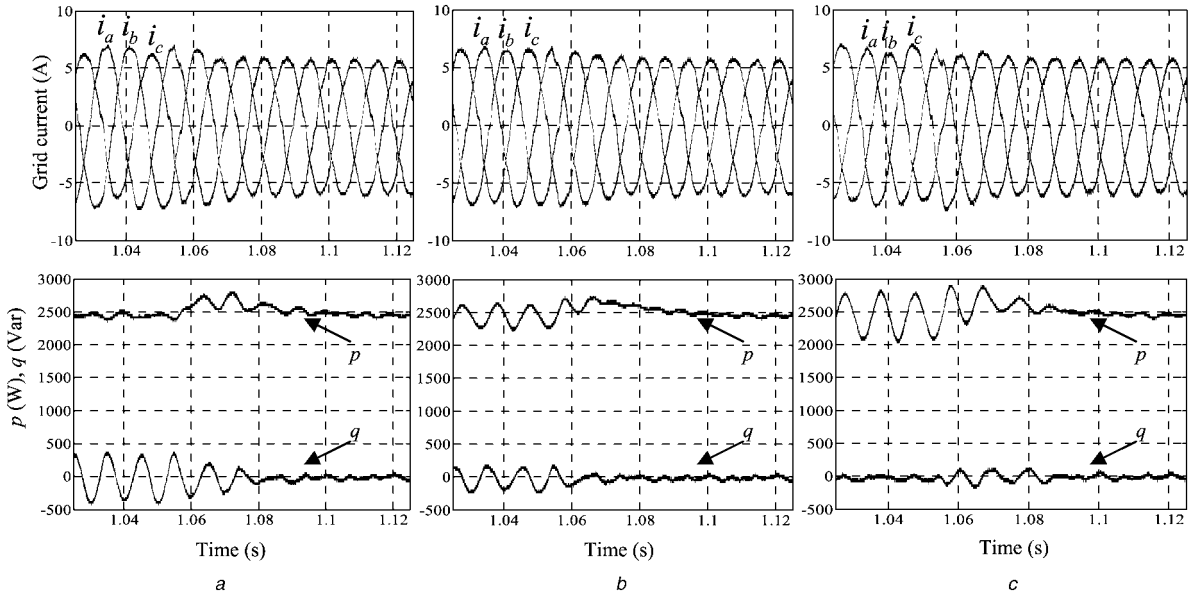

Figure 10 *Experimental results when the voltage recovers at $t = 1.055$ s, where the waveforms from top to bottom are injected grid currents and instantaneous power*

a With $k_p = -1$
b With $k_p = 0$
c With $k_p = 1$

power are equal in amplitude and have a 90^0 phase shift, as only positive-sequence currents exist. The results when $k_p = 1$ are given in Fig. 8*c*, it can be seen that the three-phase currents are in phase with the corresponding voltages. This means that unity power factor can be achieved. In addition, dc-voltage ripples during voltage dips are also observed as shown in Fig. 9, where the ripples reflected by the ac-side oscillating active power are clearly illustrated. Note that the dc-voltage variations are not large, even when $k_p = 1$, because of the big dc-link capacitance used in the system and relatively low tested power.

5.2.2 After voltage dips: Experimental results are also measured when grid voltages recover after voltage dips. As shown in Fig. 7*b*, the unbalanced grid voltages become balanced at $t = 1.055$ s. With respect to different values of k_p, corresponding results of injected grid currents and instantaneous power are shown in Fig. 10. It can be seen that different current waveforms and instantaneous power waveforms, which were controlled by k_p under voltage dips, are the same as originally when the grid voltages become balanced.

6 Conclusion

This paper has proposed a generalised active power control strategy for DG inverters operating under unbalanced grid faults. Based on derived formulas and graphic representations, the contributions of symmetric-sequence components to the instantaneous power and the interactions between symmetric sequences have been explained in detail. By intentionally introducing an adjustable parameter in between the reference currents and the grid voltages, a strategy has been found to be able to control the dc-link ripples, the symmetry of currents or the power factors in terms of controllable oscillating active and reactive powers. Then the analysis of strategy applications from the perspective of both the power-electronic converters and the power system were discussed. The flexible adaptivity of the proposed strategy allow it to cope with multiple constraints in practical applications. Finally, the proposed control strategy was tested based on an experimental system, and the measured results verified the performance as expected. The next-step work is going further with on-line optimum control for specific DG systems based on the proposed strategies.

7 References

[1] MCGRANAGHAN M.F., MUELLER D.R., SAMOTYJ M.J.: 'Voltage sags in industrial systems', *IEEE Trans. Ind. Appl.*, 1993, **29**, (2), pp. 397–403

[2] ZHANG L., BOLLEN M.H.J.: 'Characteristic of voltage dips (sags) in power systems', *IEEE Trans. Power Del.*, 2000, **15**, (2), pp. 827–832

[3] E.O. Netz Gmbh: 'Grid Code for high and extra high voltage', 2006

[4] National Grid Electricity Transmission Plc, U.K.: 'The Grid Code', 2009

doi: 10.1049/iet-gtd.2009.0607

[5] SANNINO A., BOLLEN M., SVENSSON J.: 'Voltage tolerance testing of three-phase voltage source converters', *IEEE Trans. Power Del.*, 2005, **20**, (2), pp. 1633–1639

[6] SONG H., NAM K.: 'Dual current control scheme for PWM converter under unbalanced input voltage conditions', *IEEE Trans. Ind. Electron.*, 1999, **46**, (5), pp. 953–959

[7] SACCOMANDO G., SVENSSON J.: 'Transient operation of grid-connected voltage source under unbalanced voltage conditions'. Proc. IEEE IAS, 2001, pp. 2419–2424

[8] MAGUEED F.A., SANNINO A., SVENSSON J.: 'Transient performance of voltage source converter under unbalanced voltage dips'. Proc. IEEE PESC, 2004, pp. 1163–1168

[9] SUH Y., LIPO T.A.: 'A control scheme in hybrid synchronous-stationary frame for PWM AC/DC converter under generalized unbalanced operating conditions', *IEEE Trans. Ind. Appl.*, 2006, **42**, (3), pp. 825–835

[10] YUAN X., MERK W., STEMMLER H., ALLMELING J.: 'Stationary frame generalized integrators for current control of active power filters with zero steady-state error for current harmonics of concern under unbalanced and distorted operating conditions', *IEEE Trans. Ind. Appl.*, 2002, **38**, (2), pp. 523–532

[11] ZMOOD D., HOLMES D.: 'Stationary frame current regulation of PWM inverters with zero steady-state error', *IEEE Trans. Power Electron.*, 2003, **18**, (3), pp. 814–822

[12] TEODORESCU R., BLAABJERG F., LISERRE M., LOH P.C.: 'Proportional-resonant controllers and filters for grid-connected voltage-source converters', *IEE Proc. Electron. Power Appl.*, 2006, **153**, (5), pp. 750–762

[13] ETXEBERRIA-OTADUI I., VISCARRET U., CABALLERO M., RUFER A., BACHA S.: 'New optimized PWM VSC control stuctures and strategies under unbalanced voltage transients', *IEEE Trans. Ind. Electron.*, 2007, **54**, (5), pp. 2902–2914

[14] YIN B., ORUGANTI R., PANDA S., BHAT A.: 'An output-power-control strategy for a three-phase PWM rectifier under unbalanced supply conditions', *IEEE Trans. Ind. Electron.*, 2008, **55**, (5), pp. 2140–2151

[15] CHONG H., LI R., BUMBY J.: 'Unbalanced-grid-fault ride-through control for a wind turbine inverter', *IEEE Trans. Ind. Appl.*, 2008, **44**, (3), pp. 845–856

[16] RODRIGUEZ P., TIMBUS A.V., TEODORESCU R., LISERRE M., BLAABJERG F.: 'Flexible active power control of distributed power generation systems during grid faults', *IEEE Trans. Ind. Electron.*, 2007, **54**, (5), pp. 2583–2592

[17] AKAGI H., WATANABE E.H., AREDES M.: 'Instantaneous power theory and applications to power conditioning' (IEEE Press, 2007)

[18] PENG F.Z., LAI J.S.: 'Generalized instantaneous reactive power theory for three-phase power systems', *IEEE Trans. Instrum. Meas.*, 1996, **45**, (1), pp. 293–297

[19] ANDERSSON P.M.: 'Analysis of faulted power systems' (IEEE Press, 1995)

[20] WANG F., DUARTE J., HENDRIX M.: 'High performance stationary frame filters for symmetrical sequences or harmonics separation under a variety of grid conditions'. Proc. IEEE APEC, 2009, pp. 1570–1576

8 Appendix 1

An alternative expression in the stationary $\alpha-\beta-\gamma$ frame for the instantaneous power calculation can be derived, that is

$$p = \boldsymbol{v}\cdot\boldsymbol{i} = (\boldsymbol{v}^{+}_{\alpha\beta} + \boldsymbol{v}^{-}_{\alpha\beta})\cdot(\boldsymbol{i}^{+}_{\alpha\beta} + \boldsymbol{i}^{-}_{\alpha\beta}) + v_{\gamma}\cdot i_{\gamma} \tag{34}$$

$$q = \boldsymbol{v}_{\perp}\cdot\boldsymbol{i} = (\boldsymbol{v}^{+}_{\alpha\beta\perp} + \boldsymbol{v}^{-}_{\alpha\beta\perp})\cdot(\boldsymbol{i}^{+}_{\alpha\beta} + \boldsymbol{i}^{-}_{\alpha\beta}) \tag{35}$$

with $v_{\gamma} = \sqrt{3}v^{0}_{a}$, $i_{\gamma} = \sqrt{3}i^{0}_{a}$, $\boldsymbol{v}_{\alpha\beta}{}^{+,-} = T_{\alpha\beta}\boldsymbol{v}^{+,-}$ and $\boldsymbol{i}_{\alpha\beta}{}^{+,-} = T_{\alpha\beta}\boldsymbol{i}^{+,-}$, where

$$T_{\alpha\beta} = \sqrt{\frac{2}{3}}\begin{bmatrix} 1 & -\frac{1}{2} & -\frac{1}{2} \\ 0 & \frac{\sqrt{3}}{2} & -\frac{\sqrt{3}}{2} \end{bmatrix}$$

The orthogonal matrix transformation is

$$\boldsymbol{v}^{+,-}_{\alpha\beta\perp} = \begin{bmatrix} 0 & 1 \\ -1 & 0 \end{bmatrix}\boldsymbol{v}^{+,-}_{\alpha\beta} \tag{36}$$

9 Appendix 2

The dot product of a positive-sequence voltage vector $\boldsymbol{v}^{+}$ and a negative-sequence vector $\boldsymbol{i}^{-}$ can be calculated in the $a-b-c$ reference frame as

$$\begin{aligned}\boldsymbol{v}^{+}\cdot\boldsymbol{i}^{-} &= v^{+}_{a}i^{-}_{a} + v^{+}_{b}i^{-}_{b} + v^{+}_{c}i^{-}_{c} \\ &= V^{+}\cos(\omega t+\varphi_1)I^{-}\cos(\omega t+\varphi_2) \\ &\quad + V^{+}\cos\left(\omega t+\varphi_1-\frac{2}{3}\pi\right)I^{-}\cos\left(\omega t+\varphi_2+\frac{2}{3}\pi\right) \\ &\quad + V^{+}\cos\left(\omega t+\varphi_1+\frac{2}{3}\pi\right)I^{-}\cos\left(\omega t+\varphi_2-\frac{2}{3}\pi\right) \\ &= \frac{3}{2}V^{+}I^{-}\cos(2\omega t+\varphi_1+\varphi_2)\end{aligned} \tag{38}$$

where symbols φ_1 and φ_2 are the phase angles of v^{+}_{a} and i^{-}_{a},

respectively. It can be seen that the dot product of $\boldsymbol{v}^+$ and $\boldsymbol{i}^-$ leads to an instantaneous power oscillations at twice the fundamental frequency.

As defined in Section 3, $\boldsymbol{i}_p^+$ and $\boldsymbol{i}_p^-$ are in phase with $\boldsymbol{v}^+$ and $\boldsymbol{v}^-$, respectively. Thus $\boldsymbol{i}_p^+ = k_1\boldsymbol{v}^+$, $\boldsymbol{i}_p^- = k_2\boldsymbol{v}^-$, where $k1$ and k_2 are scalars. Hence, we can obtain

$$\boldsymbol{v}^- \cdot \boldsymbol{i}_p^+ = \frac{1}{k_2}\boldsymbol{i}_p^- \cdot k_1\boldsymbol{v}^+ = \frac{k_1}{k_2}(\boldsymbol{v}^+ \cdot \boldsymbol{i}_p^-) \tag{39}$$

Likewise, we can also find that the dot products of $\boldsymbol{v}_\perp^- \cdot \boldsymbol{i}_p^+$ and $\boldsymbol{v}_\perp^+ \cdot \boldsymbol{i}_p^-$ have a similar relationship.

IET Gener. Transm. Distrib., 2010, Vol. 4, Iss. 8, pp. 905–916
doi: 10.1049/iet-gtd.2009.0607